

Optimizing Ultrasonic Plus Resistance Spot Welding for Dissimilar Metal Joining

Insert material and welding parameters were optimized for reduced intermetallic thickness and improved mechanical properties of aluminum to steel joints

BY Y. LU, K. ZHANG, J. TRAN, E. MAYTON, M. KIMCHI, AND W. ZHANG

ABSTRACT

Bimetallic structures made of aluminum alloys and high-strength steels are increasingly utilized for vehicle lightweighting applications. Joints made by direct resistance spot welding (RSW) of aluminum alloy to steel commonly suffer from inferior mechanical properties due to the formation of thick and brittle intermetallic compounds as well as solidification-related defects. In our previous work, a new joining method of ultrasonic plus resistance spot welding (U + RSW) was developed to overcome the aforementioned issues in direct RSW of Al to steel. In the present study, the U + RSW process parameters were optimized for joining 1-mm-thick AA6061-T6 to 0.9-mm-thick AISI 1008 steel to achieve a high joint strength of 3.7 kN and consistent button pullout failure mode. Specifically, it investigated the effect of the insert material, ultrasonic spot welding (USW) energy, as well as RSW electrode geometry, power source, and welding time on the nugget size and mechanical properties of the dissimilar U + RSW joints. The morphology and thickness of the intermetallic layer were characterized in a scanning electron microscope. It was found that a thin layer (less than 1.4 μm) of intermetallic compounds formed at the Al/steel interface of the final joint. Wedge testing of Al/steel joints was further developed for in-situ observation of deformation and failure behavior in a coach-peel loading condition.

KEYWORDS

- Dissimilar Metal Welding • Aluminum Alloy • Steel
- Mechanical Properties • Intermetallic Compounds
- Automotive Lightweighting

Introduction

To address an increasing demand for weight reduction of vehicle structures, multimaterial design has been deployed utilizing high-strength steels for crash performance and light metals, such as aluminum alloys, for further weight reduction and corrosion resistance (Ref. 1). (Note that Al will be used as the abbreviation for aluminum alloy.) A robust dissimilar metal-joining process is essential to ensure the

quality and performance of bimetallic structures made of Al and high-strength steel. The joining of Al to steel by resistance spot welding (RSW), one of the most widely used joining methods in the automotive industry, is certainly desirable but suffers from inferior mechanical properties. Such inferior properties are primarily due to the formation of thick and brittle intermetallic compounds (IMCs) and solidification-related defects such as solidification cracking and shrinkage voids, as well as severe expulsion.

A variety of solid-state welding and mechanical fastening processes have been developed for the dissimilar metal connection of Al to steel. These processes include friction stir spot welding (Ref. 2), vaporizing foil actuator welding (Ref. 3), magnetic pulse welding (Ref. 4), and self-piercing riveting (Ref. 5). Another interesting process is ultrasonic spot welding (USW), which was used by Macwan et al. to join Al to galvanized high-strength low-alloy steel (Ref. 6). They obtained a thin (2–3 μm) intermetallic layer of FeAl_3 at the joint interface and a high joint strength of 4.3 kN. However, the application of USW to vehicle structural joining remains a major challenge due to issues such as Al sticking to welding tools as well as special requirements of fixturing or clamping. These issues are exacerbated when a high ultrasonic energy is used to join hard metals (e.g., steels).

In our previous study (Ref. 7), a new joining method that took advantage of both USW and RSW processes was developed for the dissimilar metal joining of Al to steel. Figure 1 is a schematic diagram of this process named as ultrasonic plus resistance spot welding (U + RSW). In the first step, a thin Al insert is ultrasonic spot welded with a steel sheet to create an intermediate joint. Then, in the second step, an Al sheet is resistance spot welded onto the Al insert side of the steel to create the final, primary joint.

When compared with solid-state joining processes in general, U + RSW has a significant advantage in that it makes use of the existing RSW equipment in automotive assembly plants. Unlike USW of Al sheet to steel, which would require high ultrasonic energy (e.g., 2000 J in the study by Macwan et al. (Ref. 6)), USW used to create the intermediate joint of thin Al insert to steel uses a low energy of 255 J, making it highly resistant to the tool sticking issue. When compared with direct RSW of Al sheet to steel, the intermediate joint by USW is essential in that it forms a metallurgical bond at the Al

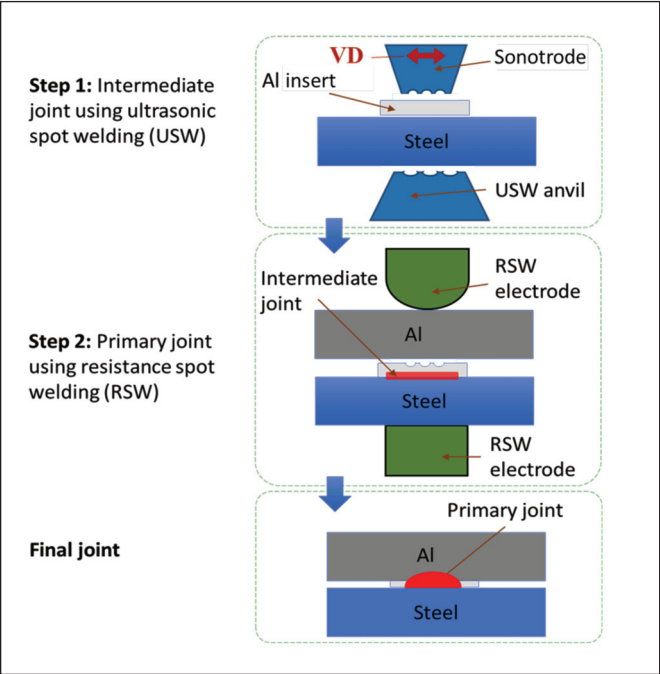


Fig. 1 — Schematic showing the U + RSW process of joining Al to steel (Ref. 7). VD is the vibration direction of the sonotrode during USW.

insert to steel interface. Such a bond in turn reduces the electrical resistance and temperature and ensuing IMC layer thickness at the interface during subsequent RSW. Our previous study showed that the final joint by U + RSW had ~ 3 times higher joint strength and ~ 6 times higher fracture energy than those by direct RSW. Finally, although a two-step process, both USW and RSW have a fast cycle time. The insert material, a commodity Al, is low cost and lightweight.

The present study expands the previous work in the following two significant ways. First, built upon the previous feasibility work, the present study investigated the effect of the insert material, USW energy, RSW electrode geometry, power source, and welding time on the nugget size and mechanical properties of the dissimilar metal joints of Al to steel created by U + RSW. Second, the testing was limited to lap-shear tensile tests in the previous work. Wedge testing of Al/steel joints is developed in this study for in-situ observation of deformation and failure behavior in a coach-peel loading condition. The new results generated in this study are essential for establishing a comprehensive understanding of processing-microstructure-property relation for dissimilar U + RSW joints.

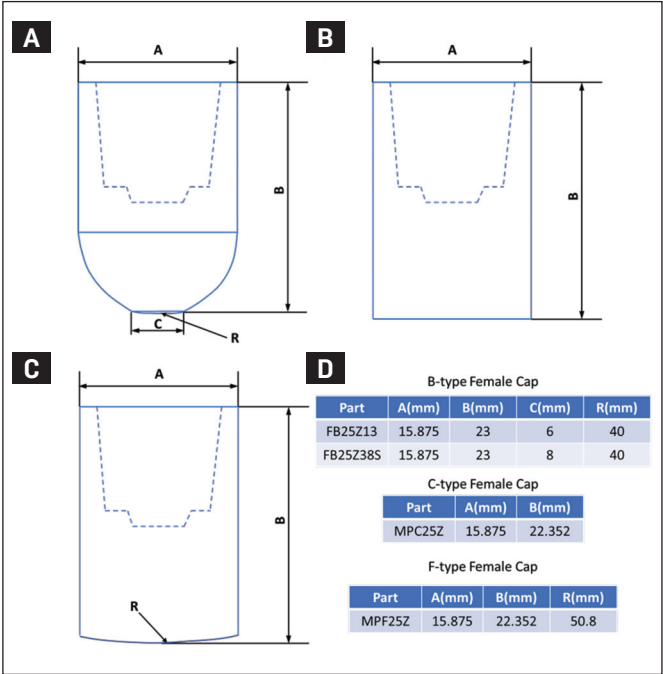


Fig. 2 — Electrode drawings of female caps: A — B-type; B — C-type; C — F-type; and D — key dimensions.

Experimental Approach

Materials

The base materials were 1-mm-thick aluminum alloy AA6061-T6 and 0.9-mm-thick cold rolled, uncoated AISI 1008 steel. Flat coupons of 100 mm in length and 38 mm in width were cut from the Al and steel sheets with the length direction aligned with the rolling direction. Two insert materials were evaluated: 0.4-mm-thick aluminum alloy AA6061-T6 and 0.3-mm-thick AA3003-H14. The nominal chemical composition along with the typical ultimate tensile strength (UTS) of these materials are summarized in Table 1.

Ultrasonic Spot Welding for Intermediate Joints

An Amtech Ultraweld® 20 2.4-kW lateral driven ultrasonic spot welding machine, designed to operate at 20 kHz with a maximum peak-to-peak amplitude of 80 μm, was used for spot welding of the Al insert to steel. The dimensions of the sonotrode tip and anvil tip were 8 × 6 mm and 12 × 12 mm, respectively. Both sonotrode and anvil surfaces had pyramid

Table 1 — Nominal Chemical Composition (wt-%) and Ultimate Tensile Strength (UTS) of Base and Insert Materials

Material	Thickness (mm)	Fe	Al	C	Mn	Si	Mg	UTS (MPa)
AISI1008	0.9	Bal.	—	≤ 0.1	0.3–0.5	—	—	305
AA6061-T6	1	≤ 0.7	Bal.	—	<0.15	0.4–0.8	0.8–1.2	310
AA3003-H14	0.3	≤ 0.7	Bal.	—	1–1.5	≤ 0.6	—	152
AA6061-T6	0.4	≤ 0.7	Bal.	—	≤ 0.15	0.4–0.8	0.8–1.2	310

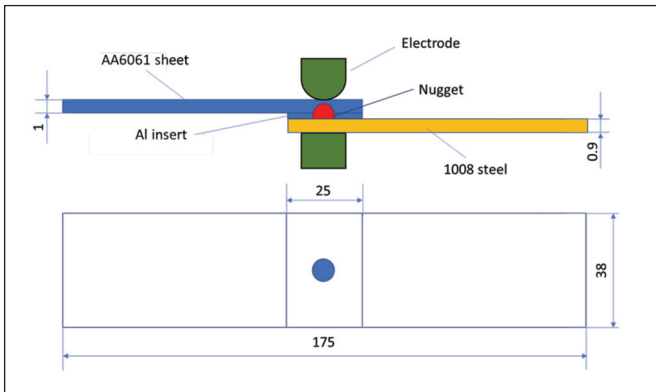


Fig. 3 — Sample geometry for lap-shear tensile testing (dimensions in mm).

knurl patterns to facilitate a firm gripping of the coupons. The vibration direction (VD) of the sonotrode was parallel to the short dimension of the coupons (thus perpendicular to the rolling direction). The coupons were ground with 240-grade sand paper and cleaned by ethanol before welding.

The USW parameters for intermediate joints, developed based on those used previously (Refs. 7, 8), are listed in Table 2. These parameters resulted in the highest tensile shear strength (TSS) of the intermediate joint, indicating a strong metallurgical bond of the Al insert to steel. The maximum TSS of ultrasonic spot welded AA3003 and AA6061 to 1008 steel were approximately 0.56 and 1.5 kN, respectively.

Resistance Spot Welding for Primary Joints

As shown in Fig. 1, the 1-mm-thick Al sheet was resistance spot welded onto the Al insert side of the steel to create the primary joint. Two RSW machines were evaluated: 1) a single-phase, 60-Hz alternating current (AC) welding machine, and 2) a medium-frequency direct current (MFDC) welding machine. Both AC and MFDC resistance spot welding machines are commonly used in the automotive industry. The RSW parameters were the following: electrode force = 3.56 kN and welding time = 5 cycles (83 ms). Such a short welding time was used to help reduce the intermetallic thickness and electrode wear; the latter was due to the alloying between the Al sheet and copper (Cu) electrode.

For electrode optimization, the electrodes tested on the Al side included a B-type, dome-shaped FB25Z13 with a 6-mm face diameter and an F-type, radius-faced electrode. The electrodes tested on the steel side included a C-type, flat electrode with a surface diameter of 15.875 mm and a B-type, dome-shaped FB25Z38S with a face diameter of 8 mm. These electrodes are schematically shown in Fig. 2A–C with the major dimensions of each type shown in Fig. 2D. For each welding con-

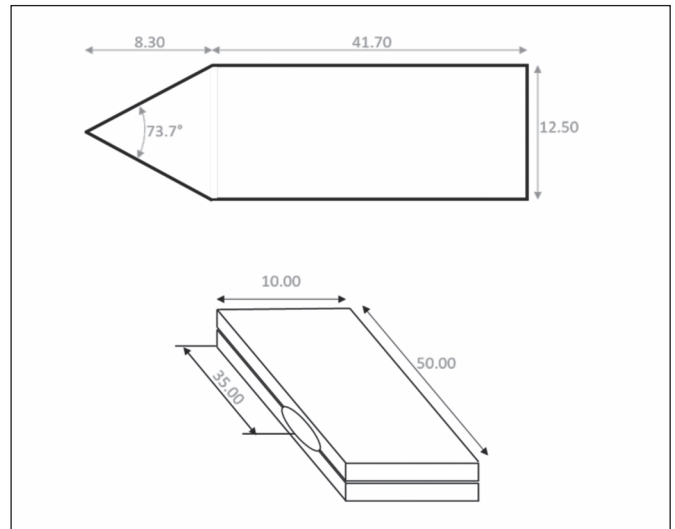


Fig. 4 — Geometry of the wedge and sample used for single-sided wedge testing (dimensions in mm).

dition, a set of four samples was welded, of which three welds were used for lap-shear tensile testing and the remaining one for microstructure characterization. Some additional specimens were also welded for wedge testing.

Microstructure Characterization

The welded samples for interfacial microstructure characterization were cross sectioned through the weld centerline. The cross-sectioned spot welds were cold mounted with epoxy to prevent aging of aluminum alloys during hot mounting. Then the samples were ground with sand papers, polished with 3- and 1- μ m diamond paste, and finished with a final vibratory polish using 0.05- μ m colloidal silica for 1 h. The IMCs at the Al/steel interface and the fracture surface were analyzed in the scanning electron microscope (SEM) with energy dispersive spectroscopy (EDS). Additionally, the cross sections of dissimilar metal welds were chemically etched with Keller's reagent (2 mL HF (48%) + 3 mL HCL + 5 mL HNO₃ + 190 mL H₂O) for Al and 2% Nital for 1008 steel. The nugget sizes were observed in an optical microscope.

Mechanical Testing

Lap-Shear Tensile Testing

The basic mechanical properties of the spot welds were tested by lap-shear tensile testing, and the geometry of the test specimen is shown in Fig. 3. Not shown in this figure is the centering shims (or spacers) added to the grip portion to

Table 2 — Ultrasonic Spot Welding Parameters for Intermediate Joints of Al Insert to Steel

Insert Material	Vibration Amplitude (μ m)	Normal Force (kN)	Energy (J)
AA6061-T6	50	1.76	255–275
AA3003-H14	40	0.88	170

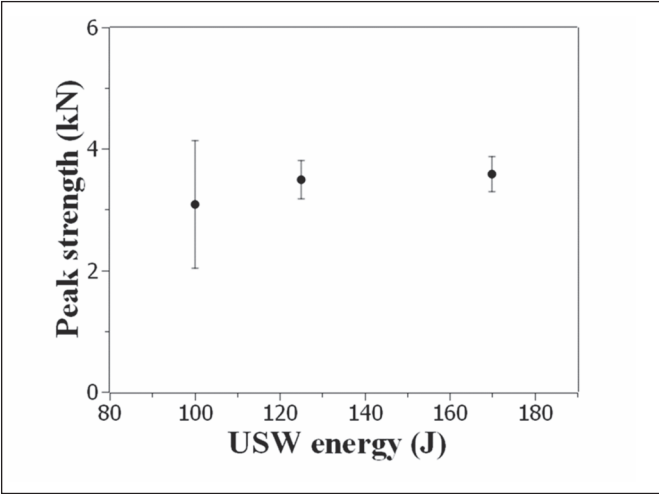


Fig. 5 — Effect of intermediate joint quality on peak strength of the final U + RSW weld for AA3003 as the insert.

align the joint with the test axis. Quasi-static lap-shear tensile testing was performed using an MTS 810 tensile testing machine with a displacement rate of 1 mm/min. The peak load was determined by the average of three samples per welding condition.

Wedge Testing

To in-situ observe the strain localization, crack initiation, and propagation in the coach-peel loading condition, a single-sided wedge test was used for testing dissimilar Al/steel joints welded by U + RSW. The dimensions of the wedge and the sample are shown in Fig. 4. The procedure of single-sided wedge testing with digital image correlation (DIC) was the same as that used previously for resistance spot welded steel sheets, for which the details are available in Ref. 9. Therefore, only the unique features of the testing setup for dissimilar Al/steel joints are highlighted in the following. In the test, one side of the sample was clamped by the fixture, while the wedge was inserted at the Al sheet/Al insert interface on the other side and then gradually pushed inward with a displacement rate of 2.5 mm/min. To investigate the effect of welding current on coach-peel fracture behavior, three welding currents were used: 17, 19, and 20 kA.

Results and Discussion

Table 3 summarizes the various process parameters of U + RSW that were investigated. Due to limited material availability,

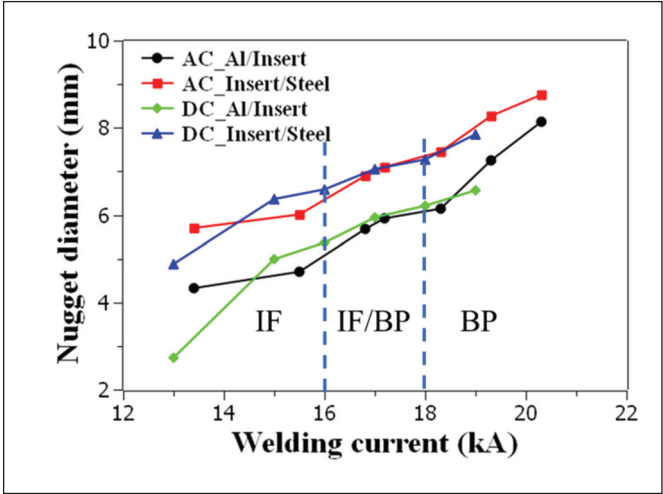


Fig. 6 — Effect of the RSW power source on the nugget diameter at Al/insert and insert/steel interfaces. AC and DC are the AC and MFDC spot welding machines, respectively. IF and BP represent interfacial and button pullout fracture modes, respectively. Insert material = AA6061-T6, electrode force = 3.56 kN, and welding time = 200 ms.

Al insert thickness was not evaluated. In addition, given that the objective was to understand the first order effect of individual variables, a design of experiment procedure was not used and the interactions between the variables were thus not obtained. Detailed results of individual variables are provided and discussed in the following sections.

Quality of Intermediate Joint

Figure 5 shows the effect of the intermediate joint quality on the TSS of the primary joint. These welds were created with the dome-shaped electrode on steel side, F-type electrode on Al side, and AA3003 as the insert. With low ultrasonic energy of 100 J for joining the intermediate joint, the average TSS of the primary joint was 3.1 kN. However, a large variation in TSS of the primary joints indicated some inconsistency of the intermediate joint quality. Moreover, expulsion was observed at the Al insert/steel interface during RSW. When the ultrasonic energy was above 125 J, the effect of ultrasonic energy on the primary joint strength was significantly reduced. A consistent nugget pullout failure mode was observed with a peak load of 3.5 kN. Thus, the metallurgical bond formed in USW with an energy above 125 J was sufficiently strong to reduce the electrical contact resistance at the insert/steel interface and prevent early ex-

Table 3 — Summary of Process Parameters of U + RSW

Parameter	Value
USW energy for intermediate joints	100, 125, and 170 J
RSW power source	AC and MFDC
Insert material	0.4-mm-thick AA6061-T6 and 0.3-mm-thick AA3003-H14
RSW electrode geometry on Al side	B-type, dome-shaped FB25Z13 and F-type, radius-faced electrode
RSW electrode geometry on steel side	C-type, flat electrode and B-type, dome-shaped FB25Z38S
Welding time of RSW	83 and 200 ms

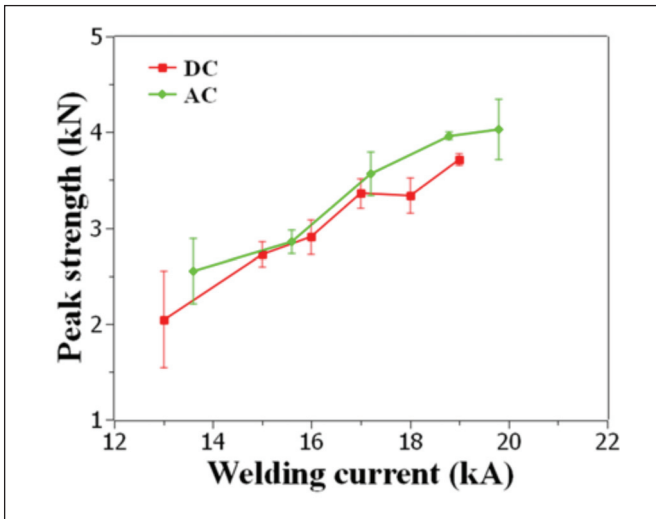


Fig. 7 — Effect of the RSW power source (AC vs. MFDC) on TSS of U + RSW joints. Welding parameters were the same as those in Fig. 6.

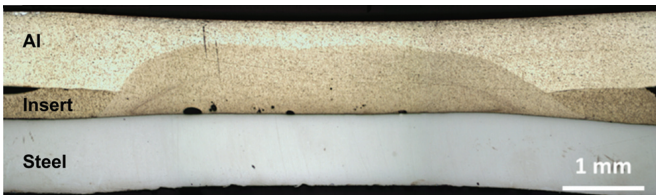


Fig. 9 — Macrostructure of the final Al/steel joint welded using an F-type electrode on the Al side and a dome-shaped electrode on the steel side. Welding current = 19 kA and welding time = 67 ms in a MFDC machine.

pulsion due to overheating locally at this interface. The negligible effect of the intermediate joint quality on the primary joint strength over a wide range of ultrasonic energy (i.e., 125 to 170 J) is essential to ensure the overall robustness of the U + RSW process.

Alternating Current vs. Medium-Frequency Direct Current Welding Machines

Figure 6 shows the nugget size at the Al/insert and insert/steel interfaces as a function of the welding current for AC vs. MFDC spot welding machines. The nugget size

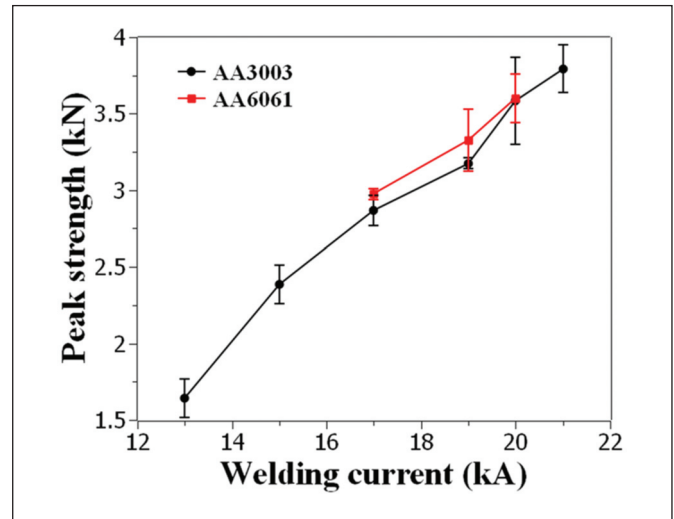


Fig. 8 — Effect of the insert material on the peak strength. Welding time = 83 ms and electrode force = 3.56 kN.

obtained in the two different types of welding machines was consistent, and it increased with increasing welding current. For the welding time of 200 ms, expulsion occurred only at a high welding current above 20 kA. Similar to the behavior shown in Fig. 6, TSS of the dissimilar metal joints was comparable between AC and MFDC welding machines at the same welding current, as shown in Fig. 7. At a welding current of 19 kA, the peak TSS was about 3.7–4.0 kN with a consistent failure mode of button pullout from the Al sheet. For this case (i.e., current = 19 kA and welding time = 200 ms), the nugget diameter at the Al/insert and insert/steel interfaces was 6.0 and 7.3 mm, respectively.

For the button pullout fracture mode, the joint strength and efficiency of the spot welds produced in AC vs. MFDC machines were calculated and summarized in Table 4. As shown in this table, there was an insignificant effect of the power source used on the joint strength and efficiency. Since MFDC machines are more widely used than AC machines in the automotive industry, the results used in the subsequent discussion are mainly for welds made in the MFDC machine.

AA6061 vs. AA3003 as Insert

The intermediate joint was resistance spot welded to the Al sheet with the electrode force of 3.56 kN and welding

Table 4 — Comparison of Joint Strength and Efficiency for Joints Produced in AC vs. MFDC Spot Welding Machines

Power Source	Welding Current and Time	Nugget Radius	TSS	Joint Strength	Joint Efficiency
MFDC	19 kA for 0.2 s	3.28 mm	3.712 kN	$\frac{3712}{2\pi \times 3.28 \times 1} = 180.1 \text{ MPa}$	$\frac{180.1}{310} = 58\%$
AC	19 kA for 0.2 s	3.62 mm	3.963 kN	$\frac{3963}{2\pi \times 3.62 \times 1} = 174.2 \text{ MPa}$	$\frac{174.2}{310} = 56\%$

*UTS of AA6061-T6 base metal was 310 MPa.

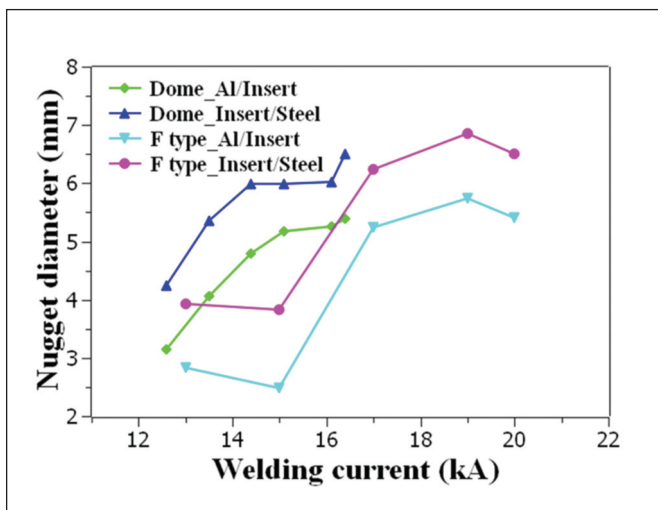


Fig. 10 — Effect of the welding current on the nugget diameter for B-type, dome-shaped vs. F-type electrodes used on the Al side.

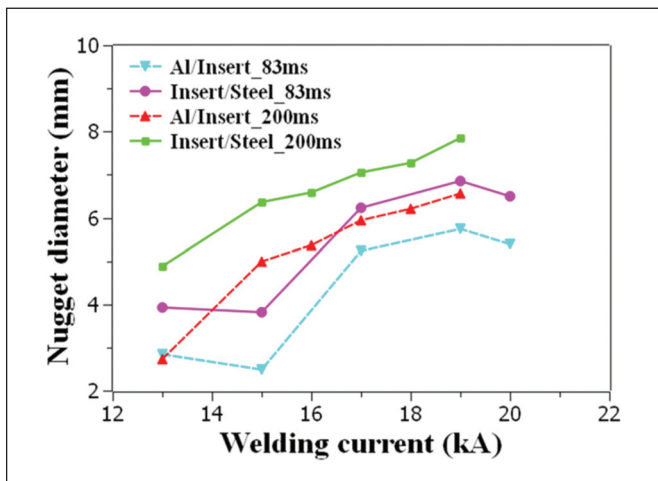


Fig. 12 — Effect of the welding time (83 vs. 200 ms) on the nugget diameter as a function of the welding current. Welds were made in a MFDC machine with 0.3-mm-thick AA3003 as the insert.

time of 83 ms in the MFDC machine. Figure 8 shows the TSS as a function of the welding current for the two different insert materials. Although the intermediate joint with AA6061 was much stronger than that with AA3003 (see “Ultrasonic Spot Welding for Intermediate Joints” in this paper), the peak strength of the final joints at various welding currents was comparable for the two insert materials. Consistent button pullout fracture was obtained at a welding current of 19 kA. Because there was no obvious advantage in the joint strength by using AA6061, and AA3003 had a lower cost than AA6061, the 0.3-mm-thick AA3003 was selected as the insert in the following tests.

Electrode Geometry

Figure 9 shows a typical macrostructure of Al/steel joint made with an F-type electrode on the Al side and a B-type,

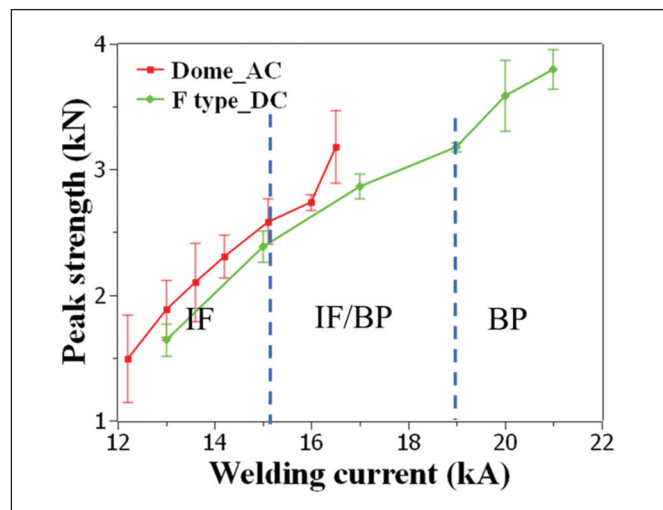


Fig. 11 — Effect of the welding current on the peak strength and failure mode for B-type, dome-shaped vs. F-type electrodes on the Al side. IF and BP designate interfacial fracture and button pullout failure modes, respectively.

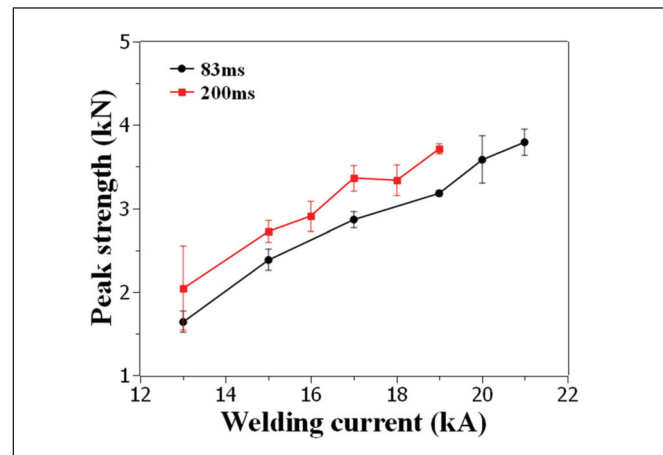


Fig. 13 — Effect of the welding time (83 vs. 200 ms) on the peak strength as a function of the welding current. Welds were made in a MFDC machine with 0.3-mm-thick AA3003 as the insert.

dome-shaped electrode on the steel side. In this case, the steel bulged into aluminum, and the bulge height increased with increasing welding current. Such bulge, resulting in an expanded area of locking, was expected to be beneficial to the strength of the weld in lap-shear tensile testing, according to Chen et al. (Ref. 10). Moreover, Fig. 9 did not show any remnant of the intermediate joint produced by USW, indicating it was completely engulfed by the molten Al during subsequent RSW.

Figure 10 shows the effect of the welding current on the nugget diameter for joints welded using the B-type, dome-shaped vs. F-type electrodes on the Al side and AA3003 as an insert in the MFDC machine. Nugget diameters at the Al/insert and insert/steel interfaces increased gradually with increasing welding current for both types of electrodes. The dome-shaped electrode tended to result in expulsion when the current was above 17 kA and the peak joint

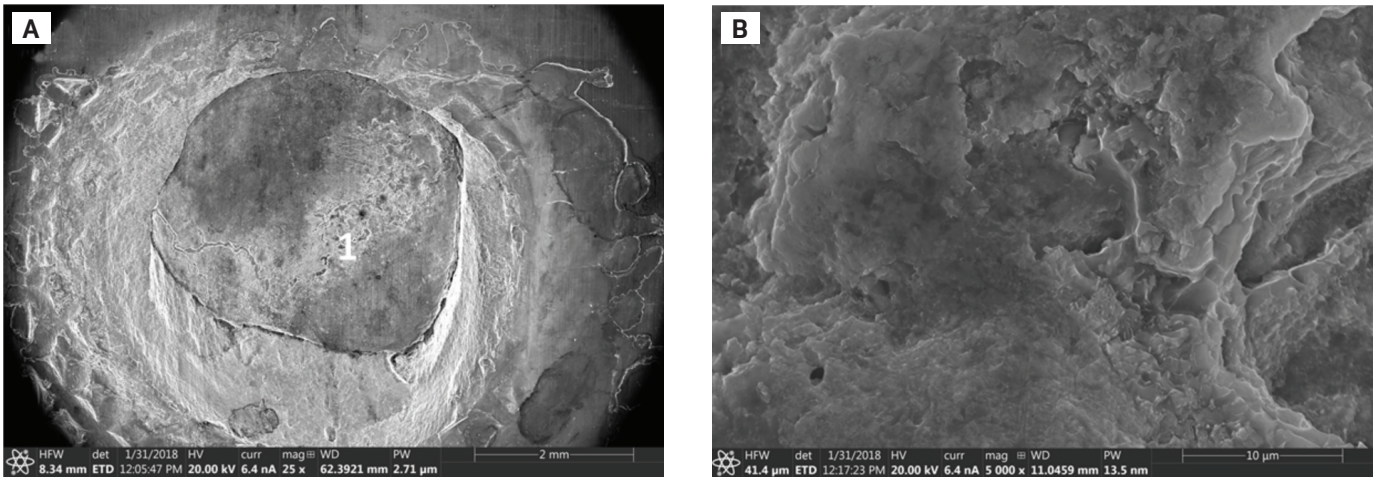


Fig. 14 — A — Macrostructure; B — zoomed-in SEM image of the IMCs formed on the top surface of the AA6061 sheet due to over-melting for the long welding time of 200 ms.

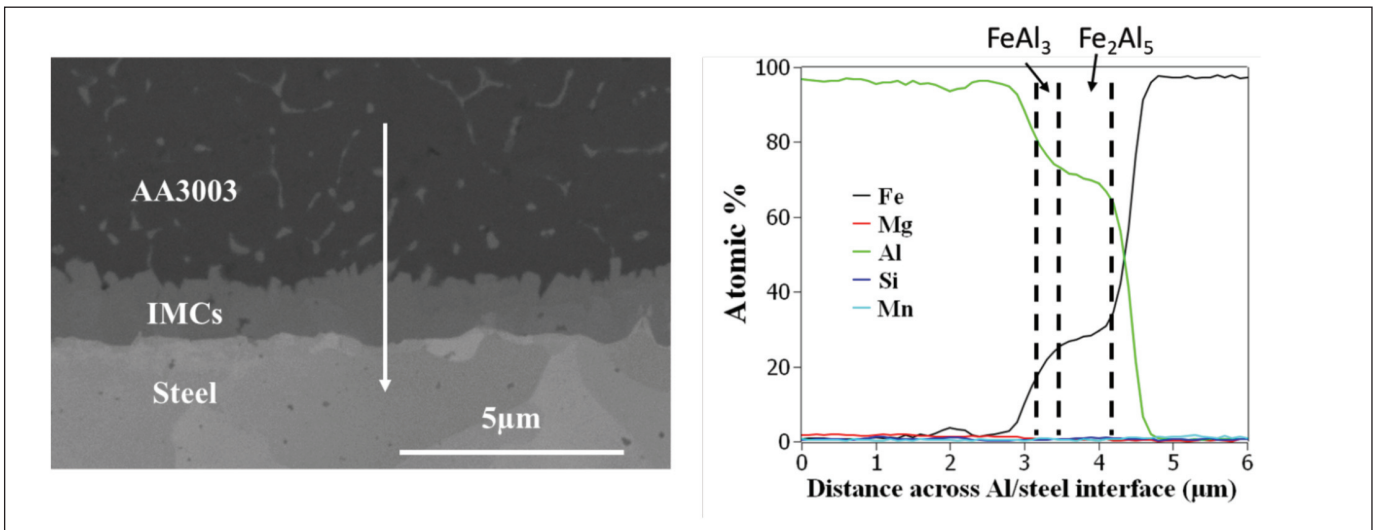


Fig. 15 — IMC morphology at the center of the final weld. Insert material was 0.3-mm-thick AA3003-H14. Welding parameters were welding current = 19 kA, welding time = 5 cycles, and electrode force = 3.56 kN.

strength was 3.2 kN at this current — Fig. 11. On the other hand, the F-type electrode did not result in a significant expulsion until the current was above 21 kA. As shown in Fig. 11, the peak joint strength for the F-type electrode at 21 kA was 3.7 kN. A possible reason for increased tolerance to expulsion in the F-type electrode is that this electrode distributed the current over a larger area at the Al sheet/insert interface, thus reducing the local current density and ensuing Joules heating. Considering the overall high joint strength and consistent button pullout failure mode, the F-type electrode was thus chosen as an improved geometry over the dome-shaped electrode used on the Al side.

Welding Time of RSW

It is generally expected that a short welding time is beneficial to reduce the IMC thickness by limiting the time for IMC growth. On the other hand, relatively long welding time, e.g., 200–800 ms, was used by Chen et al. (Ref. 10) for RSW of Al to steel. In this section, the results obtained for a short weld-

ing time of 83 ms and a relatively long welding time of 200 ms were compared. As shown in Fig. 12, the nugget diameter at both Al/insert and insert/steel interfaces increased with increasing welding time for the same welding current, as expected. At a welding current of 19 kA, the nugget diameters at the Al/insert and insert/steel interfaces were 6.56 and 7.845 mm, respectively, for the welding time of 200 ms. These diameters were about 21.5 and 8.7% larger than those welded with a welding time of 83 ms. Corresponding to a larger nugget diameter, the peak strength of the spot welds with a welding time of 200 ms was higher than that of 83 ms at the same current, as shown in Fig. 13. For instance, at a welding current of 19 kA, the peak strength of the spot welds with a welding time of 200 ms was 3.71 ± 0.06 kN, which was 0.54 kN higher than that with a welding time of 83 ms. For the welding time of 200 ms, consistent nugget pullout failure was obtained when the welding current was equal to or higher than 18 kA. For the welding time of 83 ms, the threshold welding current for obtaining consistent nugget pullout failure was slightly higher at 19 kA.

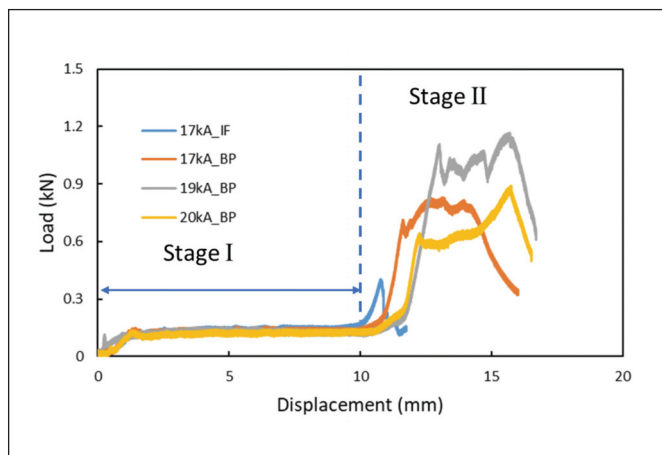


Fig. 16 — Load displacement curves for single-sided wedge testing of joints welded at different welding currents. IF is the interfacial failure, and BP is the button pullout from the Al sheet.

Severe melting of the top surface of the Al sheet occurred for the long welding time of 200 ms, which could result in rapid electrode degradation due to the alloying of aluminum with copper (Cu) electrode. A typical overmelted aluminum surface is shown in Fig. 14. Based on EDS analysis, Al_2Cu formed due to the alloying of Cu with aluminum sheet. On the other hand, overmelting did not occur with the welding current of 21 kA for the short welding time of 83 ms. At the same time, the peak TSS reached the same level as that joined with the long welding time of 200 ms (see Fig. 13). Overall, the short welding time (83 ms or 5 cycles) was found to produce better weld quality with high peak load, low electrode deterioration, and small porosity than the long welding time of 200 ms.

Microstructure at the Interface of Al Insert to Steel in the Primary Joint

In general, Fe-Al IMCs form at the Al/steel interface due to the limited solubility of iron in aluminum. The morphology of IMCs formed after U + RSW with 0.3-mm-thick AA3003-H14 insert is shown in Fig. 15. An up-to-1.4- μm -thick IMC layer was observed at the weld center with a flat interface on the steel side, while needle-like shaped IMCs grew into the Al sheet. The Fe and Al distributions across the insert/steel interface indicate that the formation of the IMCs was mainly controlled by interdiffusion of Fe and Al across the interface of liquid Al and solid steel (Ref. 11). Based on EDS analysis results, the IMCs formed at the Al/steel interface were likely Fe_2Al_5 and FeAl_3 adjacent to the steel and Al insert, respectively.

Wedge Testing

For single-sided wedge testing, the load-displacement curves of welds with different welding currents are shown in Fig. 16. Two stages can be observed in those curves. In Stage I, the force gradually increased from 0 to 0.123 ± 0.013 kN as the insertion displacement increased initially to 1–1.5 mm. Then the force was steady at 0.123 kN until around 10 mm, at

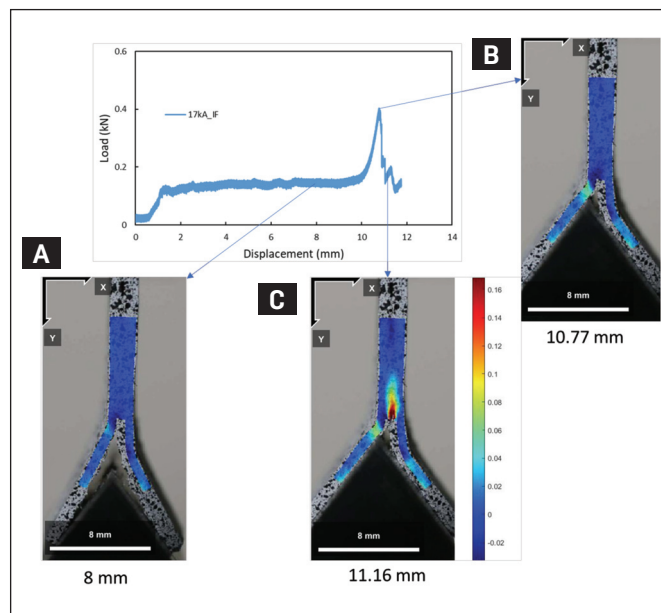


Fig. 17 — Strain (ϵ_{xx}) distribution for a joint failed by interfacial fracture at three insertion displacements: A — 8 mm; B — 10.77 mm; C — 11.16 mm. The left leg is the Al sheet, and the right leg is the insert and steel. Welding current was 17 kA.

which the tip of the wedge was fully inserted between the Al sheet and Al insert. In Stage II, the force rapidly increased from 0.123 kN to the peak strength as the crack initiated and propagated. For two “duplicates” at a welding current of 17 kA, one failed by interfacial fracture at the insert/steel interface and the other by button pullout from the Al sheet (Ref. 7); the former had a much lower joint strength. With an increasing welding current above 19 kA, the failure modes were consistent button pullout from the Al sheet.

For the aforementioned joint failed by interfacial fracture, Fig. 17 shows the strain (ϵ_{xx}) distribution measured by DIC at different displacements in the load-displacement curve. In Stage I (displacement = 8 mm), the wedge was inserted between the Al sheet and insert, bending both the Al sheet clockwise and the Al insert and steel sheet counter-clockwise. As shown in Fig. 17A, a small strain localization was observed near the periphery of the electrode indentation on the Al sheet. No obvious strain localization was observed at the Al/insert notch. At the peak load (displacement = 10.77 mm) in Stage II, strain localization was clearly observed at the Al sheet (left leg) due to the tip of the wedge in contact with the Al sheet, as shown in Fig. 17B. Posttest examination revealed a crack initiated at that location of contact and propagated in the Al sheet. However, as the wedge was inserted further, the strain localized at the Al/insert notch quickly reached a maximum value of 0.16, as shown in Fig. 17C. As a result, the second crack was initiated at this notch and propagated along the IMC layer at the Al insert/steel interface leading to the final interfacial failure.

From the results in Fig. 17, it is deduced that the final failure resulted from the following two competing cracking mechanisms as shown in Fig. 18: 1) the strain accumulation and necking at the Al sheet, and 2) the stress concentration at the Al/insert notch. The final failure depends on the low-

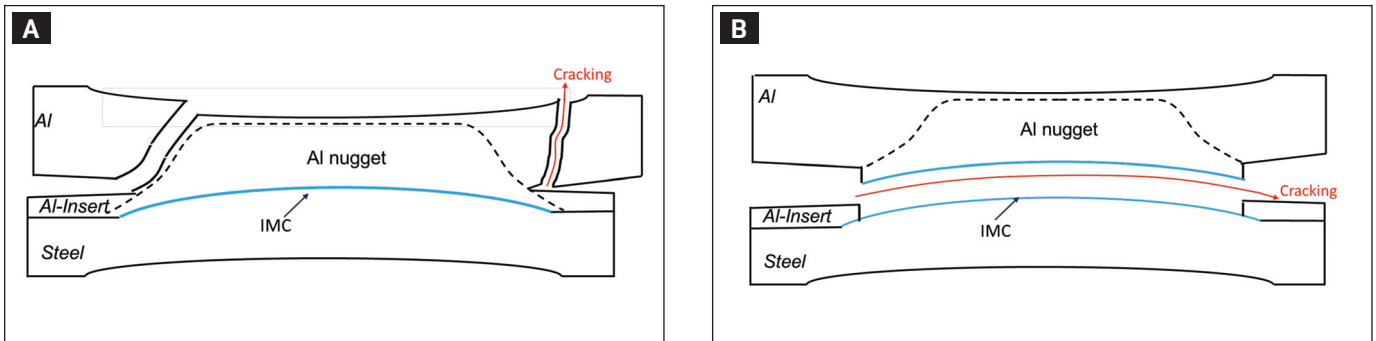


Fig. 18 — Schematics of two competing failure mechanisms: A — Button pullout; B — interfacial fracture.

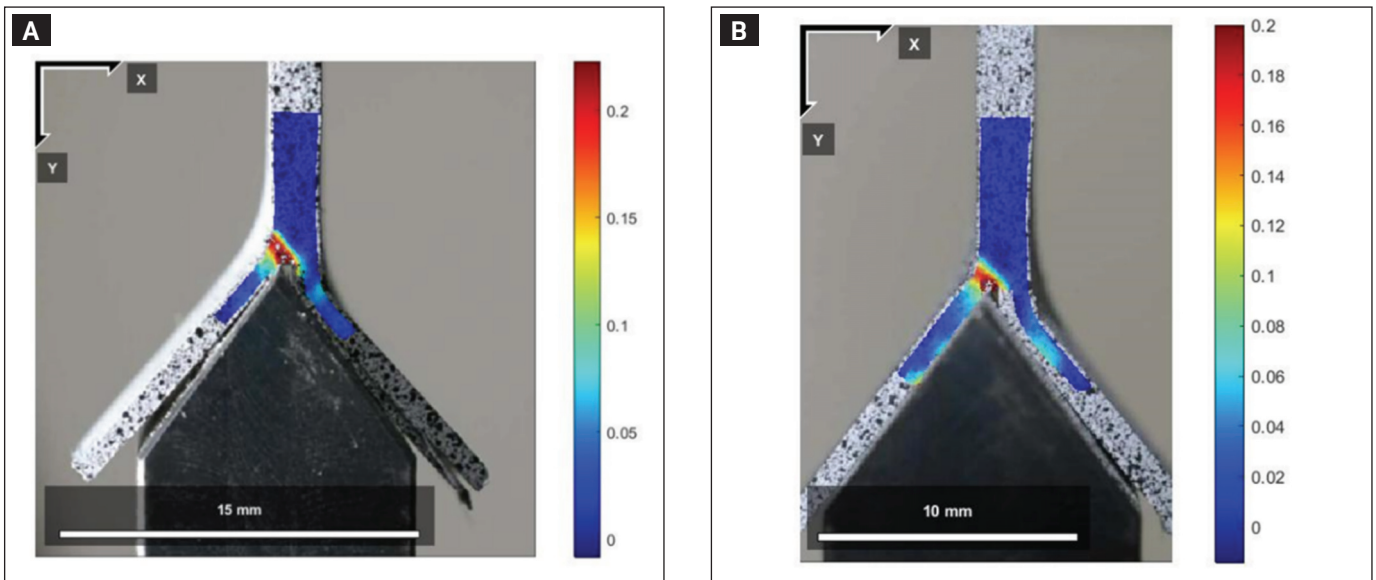


Fig. 19 — Strain (ϵ_{xx}) distribution for button pullout failure mode with a welding current of the following: A — 19 kA; B — 20 kA.

er force required for the two competing mechanisms. At a welding current of 17 kA, such competing forces were likely comparable, thus resulting in the variability in failure mode (i.e., either interfacial or button pullout). As the welding current was further increased to 19 and 20 kA, the nugget size was sufficiently large and the indentation on the Al sheet was sufficiently high to cause consistent button pullout from the Al sheet. Under these conditions, the strain localized to the heat-affected zone near to the fusion boundary in the Al sheet, as shown in Fig. 19A and B.

Summary and Conclusions

In summary, a novel process, U + RSW, was significantly improved for dissimilar metal joining of aluminum alloy AA6061-T6 to cold-rolled 1008 steel. Particularly, the effect of welding parameters, the intermediate joint quality, as well as the insert material on mechanical properties and failure mode of the primary joint were investigated. The main conclusions are as followed:

1) A consistent failure mode of nugget pullout from the Al sheet with TSS of about 3.7 kN was obtained for the following welding parameters: 0.3-mm-thick AA3003 as an insert; F-type electrode on the Al side; B-type, dome-shaped

electrode on the steel side; welding current of 19 kA; and welding time of 83 ms. Such sound joint strength was attributed to the thin layer of IMCs (less than 1.4 μm) formed at the Al/steel interface.

2) An increase of welding time from 83 to 200 ms led to a further increase in TSS, although severe electrode wear occurred due to the overmelting of the Al sheet.

3) The nugget size and peak load for the joints welded in AC vs. MFDC machines were comparable, indicating that the U + RSW process was not sensitive to the welding power supply.

4) The TSS of primary joints was not sensitive to the intermediate joint quality over a wide range of ultrasonic welding energy of 125 to 175 J for AA3003 as an insert.

5) Single-sided wedge testing allowed in-situ observation of deformation and failure under the coach-peel loading condition. Two competing failure mechanisms were found: I) the stress and strain concentration at the Al sheet/Al insert notch responsible for interfacial fracture, and II) the stress and strain concentration through the heat-affected zone of the Al sheet responsible for nugget pullout fracture. When the welding current was equal to or above 19 kA, the second mechanism dominated, resulting in consistent button pullout from the Al sheet.

Acknowledgments

This work is funded in part by The Ohio State University Simulation Innovation and Modeling Center (SIMCenter) through support from Honda R&D Americas (HRA) Inc. The authors thank Tim Abke of HRA for the valuable discussion.

References

1. Sun, X., Stephens, E. V., Khaleel, M. A., Shao, H., and Kimchi, M. 2004. Resistance spot welding of aluminum alloy to steel with transition material — From process to performance — Part 1: Experimental study. *Welding Journal* 83(7): 188-s to 195-s.
2. Kimapong, K., and Watanabe, T. 2004. Friction stir welding of aluminum alloy to steel. *Welding Journal* 83(10): 277-s to 282-s.
3. Chen, S., Daehn, G. S., Vivek, A., Liu, B., Hansen, S. R., Huang, J., and Lin, S. 2016. Interfacial microstructures and mechanical property of vaporizing foil actuator welding of aluminum alloy to steel. *Materials Science and Engineering A* 659: 12–21. DOI: 10.1016/j.msea.2016.02.040
4. Aizawa, T., Kashani, M., and Okagawa, K. 2007. Application of magnetic pulse welding for aluminum alloys and SPCC steel sheet joints. *Welding Journal* 86(5): 119-s to 124-s.
5. Abe, Y., Kato, T., and Mori, K. 2006. Joinability of aluminium alloy and mild steel sheets by self piercing rivet. *Journal of Materials Processing Technology* 177(1–3): 417–421. DOI: 10.1016/j.jmatprotec.2006.04.029
6. Macwan, A., Kumar, A., and Chen, D. L. 2017. Ultrasonic spot welded 6111-T4 aluminum alloy to galvanized high-strength low-alloy steel: Microstructure and mechanical properties. *Materials and Design* 113: 284–296. DOI: 10.1016/j.matdes.2016.10.025
7. Lu, Y., Mayton, E., Song, H., Kimchi, M., and Zhang, W. 2018. Dissimilar metal joining of aluminum to steel by ultrasonic plus resistance spot welding — Microstructure and mechanical properties. *Materials and Design* 165: 1–11. DOI: doi:10.1016/j.matdes.2019.107585
8. Lu, Y., Song, H., Taber, G. A., Foster, D. R., Daehn, G. S., and Zhang, W. 2016. In-situ measurement of relative motion during ultrasonic spot welding of aluminum alloy using photonic doppler velocimetry. *Journal of Materials Processing Technology* 231: 431–440. DOI: 10.1016/j.jmatprotec.2016.01.006
9. Peer, A. 2017. Performance testing and modeling of ultrahigh strength steel and complex stack-up resistance spot welds. Master's thesis. The Ohio State University.
10. Chen, N., Wang, H. P., Carlson, B. E., Sigler, D. R., and Wang, M. 2017. Fracture mechanisms of Al/steel resistance spot welds in lap shear test. *Journal of Materials Processing Technology* 243: 347–354. DOI: 10.1016/j.jmatprotec.2016.12.015
11. Zhang, W., Sun, D., Han, L., Gao, W., and Qiu, X. 2011. Characterization of intermetallic compounds in dissimilar material resistance spot welded joint of high strength steel and aluminum alloy. *ISIJ International* 51(11): 1870–1877. DOI: 10.2355/isijinternational.51.1870

YING LU, KAIWEN ZHANG, JOLENE TRAN, ELLIS MAYTON, MENACHEM KIMCHI, and WEI ZHANG (zhang.3978@osu.edu) are with the Department of Materials Science and Engineering, The Ohio State University, Columbus, Ohio. MAYTON is also with Welding Technology Corp., Farmington Hills, Mich.



American Welding Society

Authors: Submit Research Papers Online

Peer review of research papers is now managed through an online system using Editorial Manager software. Papers can be submitted into the system directly from the *Welding Journal* page on the AWS website (aws.org) by clicking on “submit papers.” You can also access the new site directly at editorialmanager.com/wj/. Follow the instructions to register or log in. This online system streamlines the review process, and makes it easier to submit papers and track their progress. By publishing in the *Welding Journal*, more than 70,000 members will receive the results of your research.

Additionally, your full paper is posted on the American Welding Society website for FREE access around the globe. There are no page charges, and articles are published in full color. By far, the most people, at the least cost, will recognize your research when you publish in the world-respected *Welding Journal*.



American Welding Society

Reprints

Custom reprints of *Welding Journal* articles, in quantities of 100 or more, may be purchased from Jill Kaletha, national account executive, Mossberg & Co. at (800) 428-3340, ext. 149, or (574) 289-9253, ext. 149.

You can also send an email to jkaleta@mossbergco.com